Swift XRT Response Matrix Files (v7)

XRT-LUX-CAL-108

Release Version: RMF-LUX-7.0
Release Date: 18 April 2005

Andrew Beardmore[1], Olivier Godet, Tony Abbey, Julian Osborne, Kim Page
University of Leicester

1 Introduction

This note describes release v7.0 of the Swift XRT response matrices. Response Matrix Files (RMFs) are released for each spectral mode of the XRT (photon counting mode, windowed timing mode and photodiode mode), for a variety of useful event pattern selections. Non-event recognition responses, which are suitable for use with the quick look TDRSS spectra, are described in a separate release note (XRT-LUX-CAL-108_TDRSS_RMF_v7).

Improvements to the RMFs with respect to the previous version (release v6.0, 15 October 2004, release note XRT-LUX-CAL-108_RMF_v6) are described below (section 4). Comparison of the RMFs with in-orbit calibration data are shown in section 5 and their limitations are addressed in section 6.

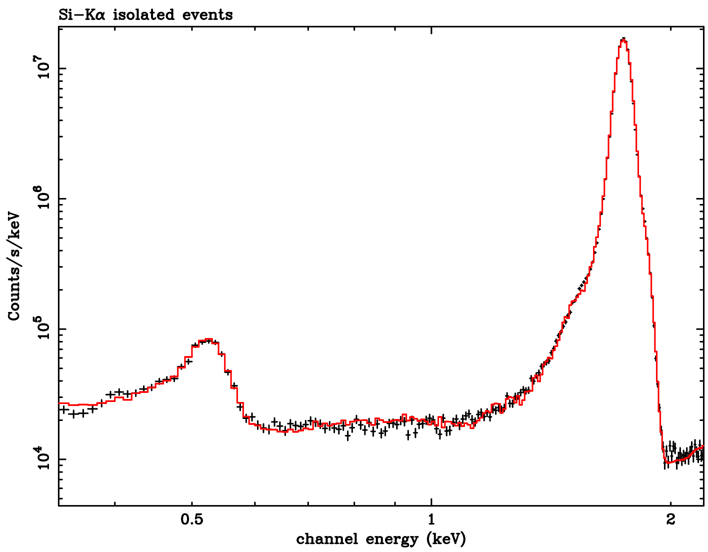

Figure 1: The XRT CCD response model is compared with an isolated event photon counting spectrum as detected by the Leicester facility with a Si-K line source. The histogram (red) shows a model consisting of Si-Kα (1.74 keV), Si-Kβ (1.84 keV), a weak O-Kα (0.525 keV) background line and an underlying bremsstrahlung continuum.

2 Response matrix generation

The RMFs are created by a Monte Carlo simulation code (Mukerjee et al., 2004). The code models the following processes: transmission of the incident X-rays through the CCD electrode structure; photo-absorption in the active layers of the device; charge cloud generation; charge cloud transportation and spreading; silicon fluorescence and associated escape peaks; surface loss effects; mapping the resultant charge cloud to the detector pixel array; charge transfer efficiency; electronic readout noise; event thresholding and classification. Figure 1 shows a fit to laboratory calibration data.

The RMFs are generated using a 5 eV input energy grid, which extends from $0-12$ keV, with 10^5 input photons per bin. The resultant spectral response is calculated over 1024 energy channels, which have a width of 10 eV per channel (the PI scale). The final RMFs were compressed with the FTOOL *cmprmf* using a threshold of 10^{-5}.

[1] apb@star.le.ac.uk

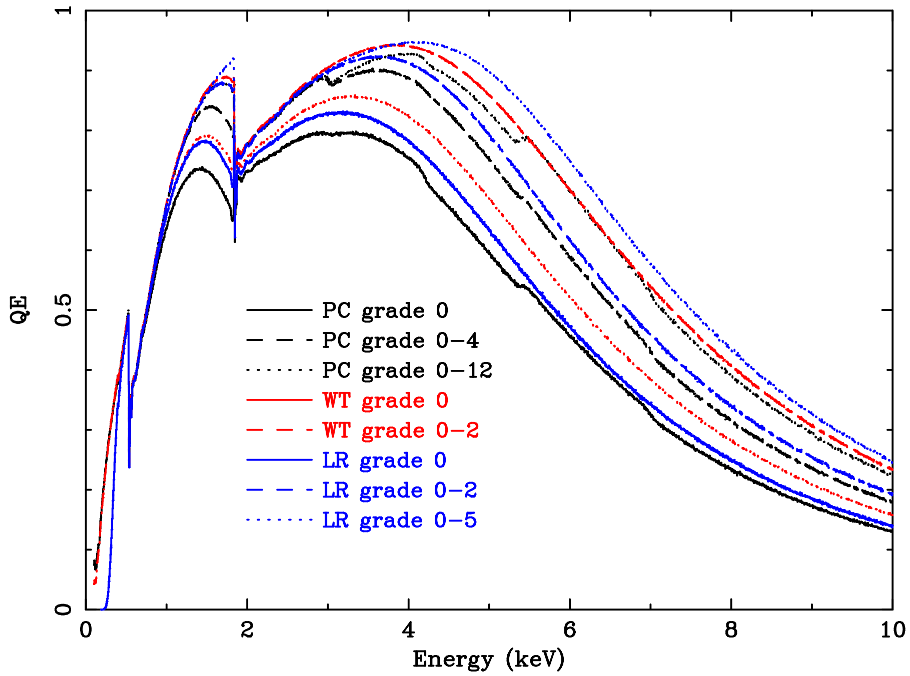

Figure 2: CCD quantum efficiency curves for the various modes and grade selection criteria for the v7 RMF release.

3 Mode dependant responses

During normal GRB observations the Swift XRT operates autonomously and acquires spectra in three modes depending on the source flux (Hill et al., 2004). These are :

(i) Photodiode mode – a fast timing mode, which is achieved by alternating the parallel and serial readouts of the CCD one pixel at a time. As a result no positional information is retained.

(ii) Window timing mode – another fast timing mode which is achieved by reading out the central 200 columns of the CCD and by binning 10 rows at a time. In this mode 1-D positional information is retained.

(iii) Photon counting mode – the traditional 2-D mode of operation for an X-ray CCD detector. In this mode a 3x3 array of pixels centered on any pixel above the event threshold is sent to the ground.

In photon counting mode X-rays are characterised by events up to 4-pixels in size depending on the energy of the incident X-ray and the corresponding depth of the initial interaction in the detector. Consequently, the quantum efficiency at higher energies is greater for larger events than isolated events, though they suffer from slightly worse spectral resolution due to additional read-noise and sub-threshold loss effects. In photodiode and window timing mode, events are translated during the readout process resulting in the requirement for different event grading schemes and response files in these modes.[2] For all three modes, event grading is performed by the ground processing software. Because the various grade selections have different advantages, RMFs are made available for a number of event grade selection criteria in each mode.

Additionally, when Swift initially slews onto a new GRB, quick-look XRT spectra are broadcast via TDRSS (the Tracking and Data Relay Satellite System) and subsequently through the GCN. These spectra will be accumulated in photodiode and/or window timing mode but have no event recognition performed — i.e. they are ungraded. We have released non-event recognition RMFs for these modes, which are described in a separate release note.

Figure 2 shows the quantum efficiency curves for the standard grade selections of the various modes, while figure 3 provides a spectral response summary.

[2]A discussion of the effects of event translation in photodiode and window timing mode can be found in Mukerjee et al. (2003), while the grading scheme for all modes is described in Burrows et al. (submitted).

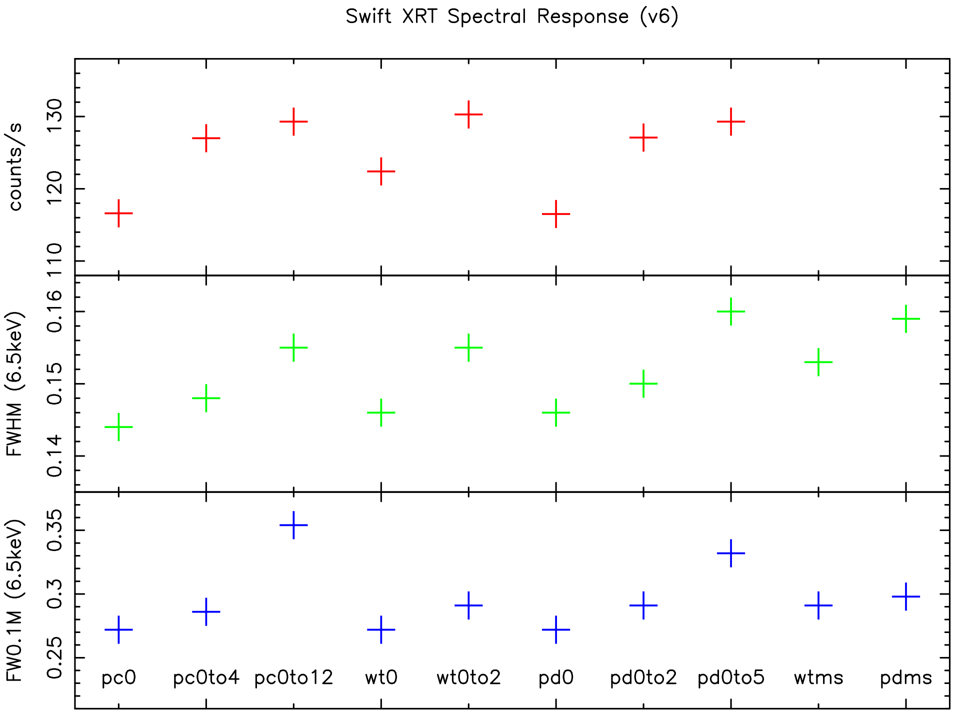

Figure 3: XRT spectral response summary for the various modes and grade selections for which RMFs have been made. The top panel shows the predicted $0.2 - 10.0\,\mathrm{keV}$ count rate of an on-axis source with a power law spectrum of photon index 2.0, absorbed by a column of $10^{21}\,\mathrm{cm}^{-2}$. The source has a band-limited unabsorbed flux of $7.0 \times 10^{-12}\,\mathrm{ergs\,cm^{-2}\,s^{-1}}$. The middle panel shows the full width at half maximum (in keV) of the response kernel at 6.5 keV, while the bottom panel shows the width at 10% of maximum. Key: PC - photon counting; WT - windowed timing; PD - photodiode; WTMS - TDRSS windowed timing; PDMS - TDRSS photodiode.

4 Changes

The previous release of the RMFs (described in release note XRT-LUX-CAL-108_RMF_v6) were based on an extensive laboratory calibration programme. The new release has been motivated partly by the continual development of the code, and also by the initial comparisons with flight data taken in the early orbit calibration phase of the mission.

4.1 Updates for v7.0

The changes for this release:

(i) X-ray interactions in the substrate have now been incorporated in the code - these give rise to large event sizes with substantial charge losses.

(ii) Improvements have been made to the surface loss functions. In particular, for PC and WT mode, the loss function formulation of Popp et al. (2000) has been applied which produces a more accurate model of the low level loss shelf seen in the internal calibration source spectra (e.g. figure 4(a) & (b), $0.6 - 1.0\,\mathrm{keV}$ & $2.0 - 3.0\,\mathrm{keV}$).

(iii) In order to reproduce the line shoulder seen in the internal calibration source for large event size spectra, the event threshold was raised to 8.5σ for PC & PD mode from the canonical 5σ value.

(iv) The modifications made to the charge cloud spreading in the last release have now been removed from the code and replaced by (iii).

(v) General code overhaul and optimisations have been made which dramatically improve the RMF generation times.

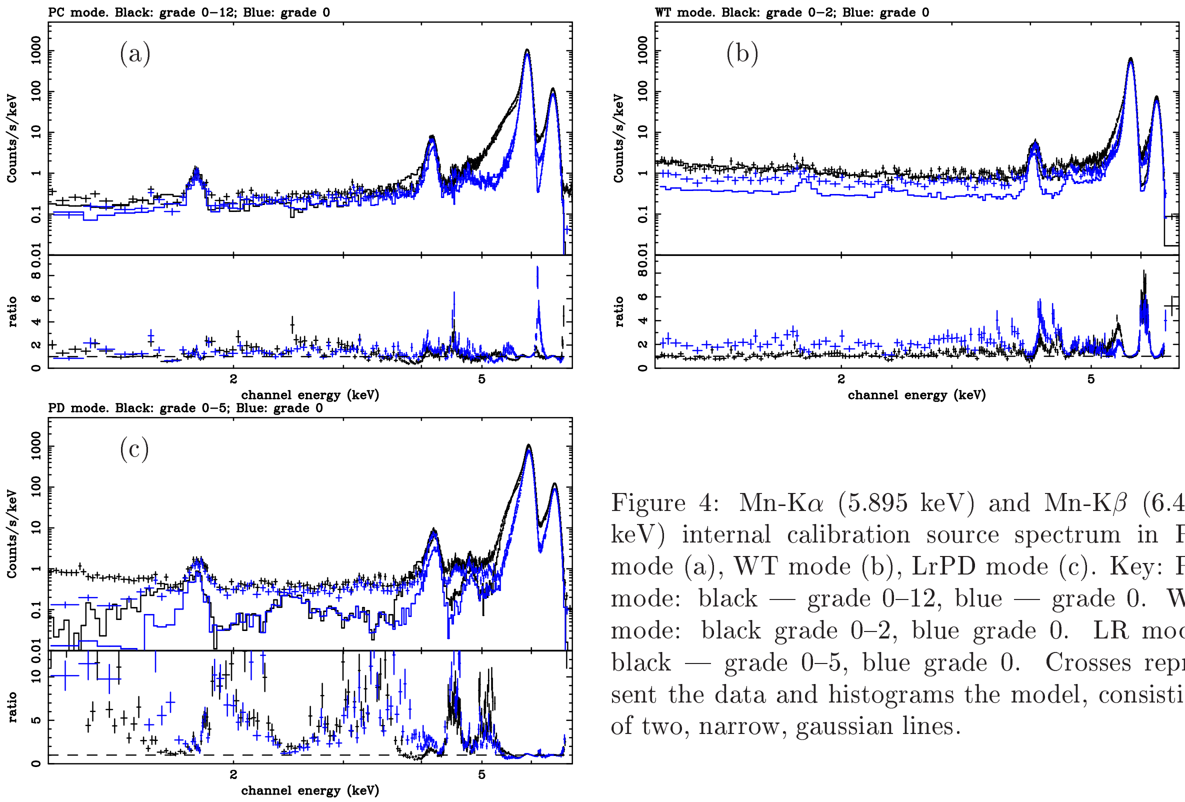

Figure 4: Mn-Kα (5.895 keV) and Mn-Kβ (6.490 keV) internal calibration source spectrum in PC mode (a), WT mode (b), LrPD mode (c). Key: PC mode: black — grade 0–12, blue — grade 0. WT mode: black grade 0–2, blue grade 0. LR mode: black — grade 0–5, blue grade 0. Crosses represent the data and histograms the model, consisting of two, narrow, gaussian lines.

5 Comparison with calibration data

Figures 4 & 5 show X-ray spectral fits made to various in-orbit calibration datasets using the released RMFs.

(i) Figure 4 shows data obtained from the on-board Fe-55 calibration source prior to the XRT door opening in the three different modes:

(a) PC mode. The RMF models the main features of the spectrum – i.e. the line core, the line shoulder, the escape peak, the Si-Kα fluorescence line and the loss-shelf – extremely well for all grade selections.

(b) WT mode. The line core and wing are well reproduced for grade 0 events, though the model starts to deviate below the 8% peak line flux level for grade 0–2. However, the loss-shelf, which exists at the level of three orders of magnitude below the main line peak, is more accurate for these larger event sizes, while it is underestimated by a factor of two for grade 0.

(c) PD mode. We find a good agreement around the line core and wing. The low level redistribution in the loss-shelf (again, three orders of magnitude below the line peak) is underestimated by a factor of a 5–10.

We emphasise these fit comparisons are based on high quality calibration data and the discrepencies between this data and the response model are well below the level reached statistically in orbit for celestial sources (see below).

(ii) Figure 5 shows spectra from a selection of in-orbit calibration targets and their best fit models.[3] These include:

(a) The Crab nebula in LrPD mode (grade 0–5). The usual model of an absorbed power law (with a photon index of 2.1, normalisation of 9.65 and column density of $3.45 \times 10^{21}\,\mathrm{cm}^{-2}$, e.g. Willingale et al. 2001) was accompanied by two additional gaussians to represent the internal corner source calibration lines which are present in this mode. The data are modelled well down to 0.7 keV, at which point residuals of 10% occur due to the ancillary response file.

[3]The default ancillary response files released with the latest Swift analysis software (XRTDAS 2, build 14) were used for these fits.

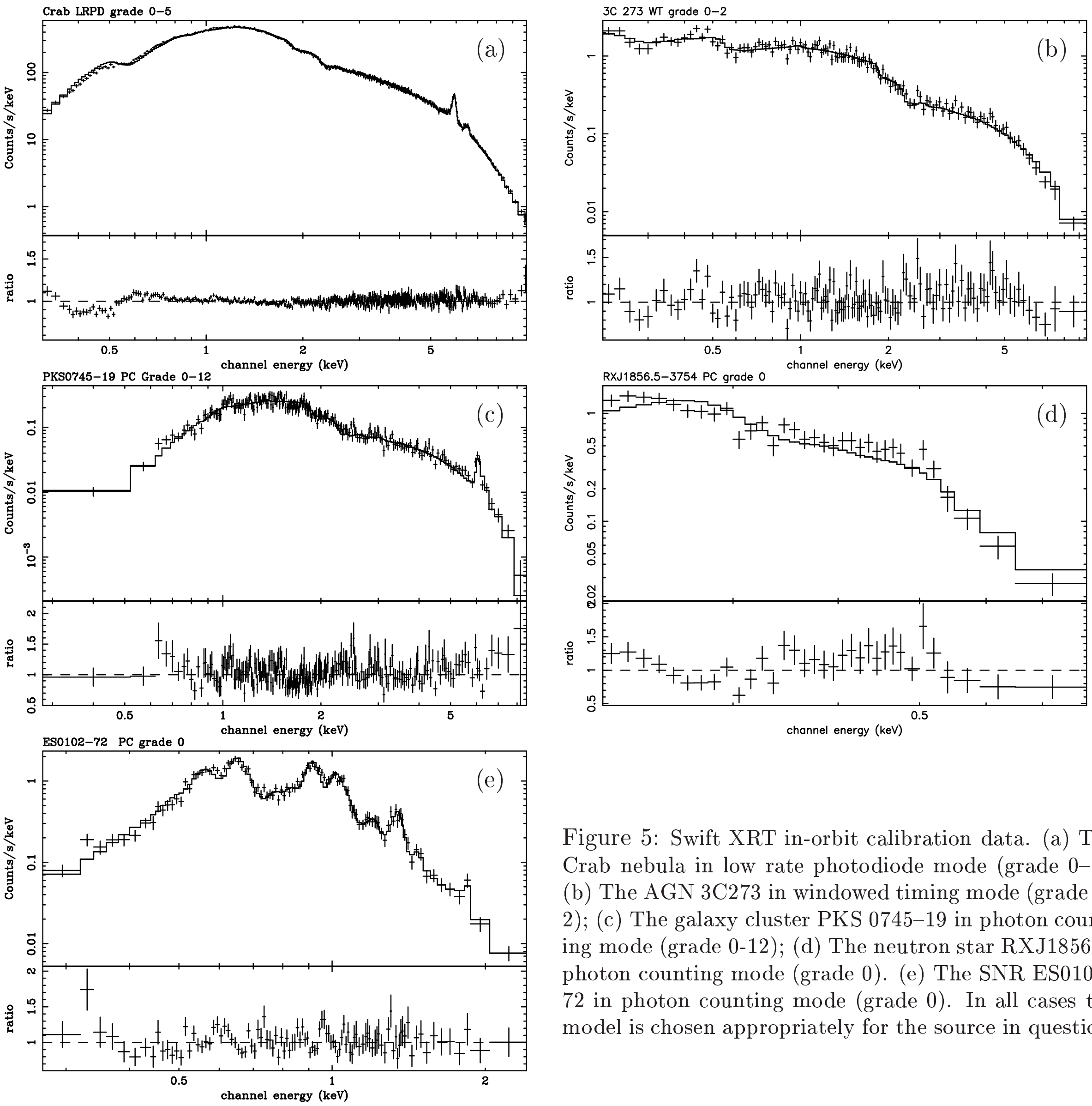

Figure 5: Swift XRT in-orbit calibration data. (a) The Crab nebula in low rate photodiode mode (grade 0–5); (b) The AGN 3C273 in windowed timing mode (grade 0–2); (c) The galaxy cluster PKS 0745–19 in photon counting mode (grade 0-12); (d) The neutron star RXJ1856 in photon counting mode (grade 0). (e) The SNR ES0102–72 in photon counting mode (grade 0). In all cases the model is chosen appropriately for the source in question.

(b) The active galaxy 3C273 in WT mode (grade 0–2). The model consists of a power law (with photon index equal to 1.58) and blackbody (temperature 60 eV), modified by galactic absorption (column density $1.79 \times 10^{20}\,\mathrm{cm}^{-2}$). The model parameters are consistent with previous observations of this source (Page et al., 2004). However, 3C273 is a variable source and we await an absolute calibration with a simultaneous observation with XMM.

(c) The galaxy cluster PKS 0745–19 in PC mode (grade 0–12). The data are modelled with a Mekal cooling flow, which had a maximum temperature of 8.8 keV, and an absorbing column density of $4.24 \times 10^{21}\,\mathrm{cm}^{-2}$. which are consistent with previous observations (e.g. Beppo-Sax, De Grandi and Molendi 1999).

(d) The neutron star RXJ1856, also in PC mode. The model consists of an absorbed 70 eV blackbody. The absorbing column density, however, was not constrained ($< 0.5 \times 10^{20}\,\mathrm{cm}^{-2}$) and is a factor of 1.8 below measurements made with the XMM RGS and Chandra LETGS instruments (Burwitz et al., 2003).

(e) The SNR ES0102 in PC mode (grade 0). The model was taken from the Chandra ACIS/ XMM-Newton cross-calibration effort (DePasquale, 2005) and consists of one fixed galactic absorption component, one variable abundance absorption component, a thermal continuum, and 20 narrow gaussian lines whose presence were determine by grating observations.

Our initial results with in-orbit calibration observations are very encouraging. However, we would urge users of Swift XRT data to probe the results of any spectral fitting for possible systematic errors by performing the analysis on the various grade selections that are available.

6 Limitations of the released RMFs

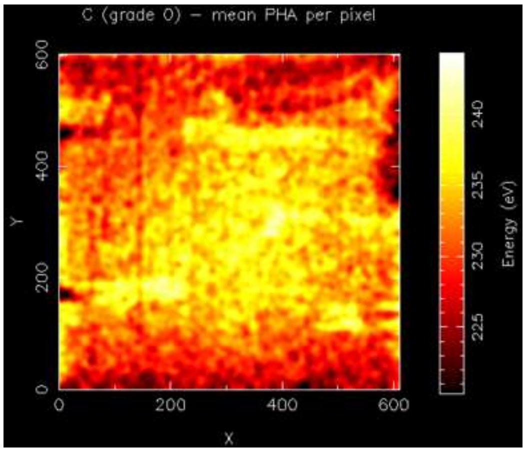

Figure 6: The spatial non-uniformity in the XRT spectral response at the lowest energies is illustrated by the average event energy for C-K illumination (0.277 keV) over the face of the detector.

(i) While we have endeavoured to make the most accurate response for the central regions of the CCD, figure 6 shows that there is a spatial gain effect at the lowest energies towards the outer regions of the detector. Spectral analysis should be performed with caution below 0.4 keV on sources in photon counting mode which appear outside the central 200×200 region of the CCD.

(ii) The photon counting mode quantum efficiencies curve (figure 2) shows discontinuities at 3.1, 4.2, 5.4 and 7.0 keV due to a slight mis-match in the loss function parameters at these boundaries. These effects are not significant for the statistical quality of astrophysical data obtained in this mode.

(iii) The default windowed timing ancillary response file released with the latest Swift XRT ftools analysis software (XRTDAS 2.0, sometimes refered to as "build 14"), can introduce an apparent oxygen edge (around 0.6 keV) in good quality data taken in this mode. An alternative ancillary response can be generated by the task xrtmkarf by using the mirror effective area file directly (see the ftools help on xrtmkarf) which is free from this problem. However, this ancillary response file can introduce residuals in the gold edge area (between $2 - 3$ keV) of order five percent. Figure 7 illustrates the differences in the fit residuals obtained using the different ancillary response files.

(iv) The RMF generator does not account for pile-up and therefore the RMFs can only reliably be used on data that is free from pile-up. This means sources which have photon counting mode count rates in excess of $\sim 0.4\,\mathrm{counts\,s^{-1}}$ should be analysed carefully using a annular extraction region to avoid the central, piled-up, regions of the XRT point spread function.

(v) While not strictly an RMF related issue, we re-emphasise that photodiode mode contains events from the entire CCD. This includes the Fe-55 calibration sources (i.e. Mn-Kα at 5.895 keV and Mn-Kβ at 6.490 keV), located at the corners of the detector. Because this is a background, rather than a response effect, the photodiode mode RMFs do not specifically take into account this emission.

7 Future developments

We continue to develop the XRT CCD response model. Future RMF releases may include:

- Improvements to the large event size response at high energies will follow once the sub-threshold loss effects are better understood and modelled.
- The model for the loss-function and loss-shelf will continue to be improved.

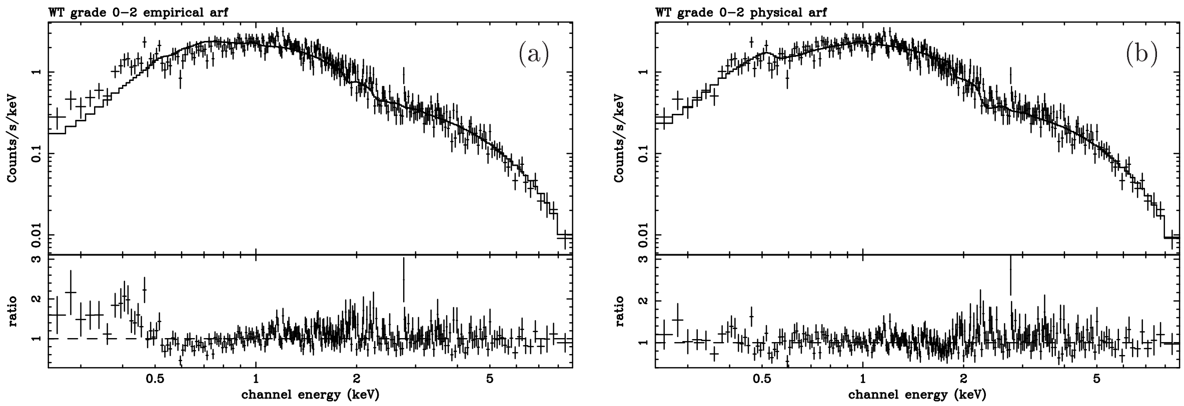

Figure 7: The spectrum and residuals obtained from windowed timing data from an anonymous GRB when it is fit with the different ancillary response files: (a) the default from xrtpipeline; (b) generated by xrtmkarf using the mirror effective area file directly.

- Off-axis RMFs with a more accurate response below 0.4 keV.
- Response model parameters tuned further to reflect in-orbit performance.
- The TDRSS non-event recognition RMF will also be updated using in-orbit measurements.

8 The RMFs released this time

swxpc0_20010101v007.rmf	PC mode grade 0
swxpc0to4_20010101v007.rmf	PC mode grade 0–4
swxpc0to12_20010101v007.rmf	PC mode grade 0–12
swxpd0_20010101v007.rmf	PD mode grade 0
swxpd0to2_20010101v007.rmf	PD mode grade 0–2
swxpd0to5_20010101v007.rmf	PD mode grade 0–5
swxwt0_20010101v007.rmf	WT mode grade 0
swxwt0to2_20010101v007.rmf	WT mode grade 0–2
swxpdmspha_20010101v006.rmf	PD mode non-event recognition (TDRSS)
swxwtmspha_20010101v006.rmf	WT mode non-event recognition (TDRSS)

REFERENCES

D.N. Burrows et al. The Swift X-ray Telescope. *Space Science Reviews*, submitted.

V. Burwitz et al. The thermal radiation of the isolated neutron star RX J1856.5-3754 observed with Chandra and XMM-Newton. *A&A*, 399:1109–1114, 2003.

S. De Grandi and S. Molendi. Spatially resolved spectroscopy of the cooling flow cluster PKS0745-191 with BeppoSAX. *A&A*, 1999.

J. DePasquale. *Chandra/ACIS - XMM/EPIC E0102 Cross-calibration page*, 2005. http://cxc.harvard.edu/acis/E0102/splash.html.

J.E. Hill et al. Readout modes and automated operation of the Swift X-ray Telescope. *Proc. SPIE*, 5165: 217–231, 2004.

K. Mukerjee, A.F. Abbey, J. Osborne, and A.P. Beardnore. Selection of the Swift XRT event pattern library and event pattern relationships. Technical Report LUX-TN-100, Leicester University, 2003.

K. Mukerjee et al. The Spectroscopic performance of the Swift X-ray Telescope for Gamma-Ray Burst studies. *Proc. SPIE*, 5165:251–261, 2004.

K.L. Page et al. XMM-Newton observations of 3C273. *MNRAS*, 349:57–67, 2004.

M. Popp et al. Modeling the energy response of pn-CCDs in the 0.2 - 10.0 keV band. *Nuclear Instruments and Methods in Physics Research A*, 439:567–574, 2000.

R. Willingale et al. New light on the X-ray spectrum of the Crab Nebula. *A&A*, 365:L212–L217, 2001.